Journal of Chemical Reviews

2026, Volume 8, Issue 3

Review Article

Computational Fluid Dynamics Guided Design of Antifouling Surface Patterned Membranes: A Review

Nafiu Umar Barambu[1,2], Sri Mulyati[1,3], Cut Meurah Rosnelly[1,3], Mohammad Roil Bilad[4], Nasrul Arahman[1,3,5,6]*

[1]*Department of Chemical Engineering, Universitas Syiah Kuala, Banda Aceh 23111, Indonesia*
[2]*Laboratory of Polymer Science, Department of Chemical Engineering, Universitas of Syiah Kuala, Banda Aceh, Indonesia, Universitas Syiah Kuala, Banda Aceh 23111, Indonesia*
[3]*Graduate School of Environmental Management, Universitas Syiah Kuala, Jl. Tgk Chik Pante Kulu No. 5, Banda Aceh 23111, Darussalam, Indonesia*
[4]*Department of Chemical Engineering, University of Brunei Darussalam, Jalan Tungku Link, Gadong BE1410, Brunei*
[5]*Research Centre for Environmental and Natural Resources, Universitas Syiah Kuala, Jl. Hamzah Fansuri, No. 4, Darussalam, Banda Aceh 23111, Indonesia*
[6]*Atsiri Research Center, Universitas Syiah Kuala, Jl. Syeh A. Rauf, Darussalam, Banda Aceh 23111, Indonesia*

Use your device to scan and read the article online

Citation: N.U. Barambu, S. Mulyati, C.M. Rosnelly, M.R. Bilad, N. Arahman, **Computational Fluid Dynamics Guided Design of Antifouling Surface Patterned Membranes: A Review**. *J. Chem. Rev.*, **2026,** *8*(3), 432-455.

https://doi.org/10.48309/JCR.2026.570067.1563

ARTICLE INFO

Received: 2026-01-01
Revised: 2026-01-25
Accepted: 2026-02-17
ID: JCR-2601-1563

Keywords:
Flow pattern design simulation, Surface patterned membranes, Antifouling membranes, Feed turbulence flow, Surface shear stress

ABSTRACT

Imposing feed turbulence flow in the membrane filtration system alleviates membrane fouling and enhances the overall membrane performance. Computational fluid dynamics (CFD) simulation provides easy access to visualizing the hydrodynamic performance of any design and technique employed for generating the membrane feed turbulence flow. Among several membrane feed turbulence flow generation techniques, membrane surface patterning and turbulence promoters are the most prominent. By patterning the surface of a membrane, the antifouling performance of the membrane improved by up to 58%. Moreover, by adjusting the operating velocity from 30 to 50 cm/s, the membrane hydraulic performance was enhanced by 20%. Furthermore, the antifouling performance of feed turbulence flow depends on operating parameters including the feed flow direction towards the turbulence generator. By reorienting the feed flow from parallel to perpendicular to the membrane surface patterns, the membrane lifespan improved by up to 14.4%. Therefore, for several decades many authors explored CFD to simulate the performance of the feed turbulence generation techniques prior to validation to save costs, time, and to obtain optimum design and operating parameters. Thus, many authors reviewed the CFD simulation results of the hydrodynamic performance of turbulence promoters while ignoring that of the surface patterning technique. This study aims to review the CFD simulation results of the hydrodynamic performance of membrane surface patterning by examining the patterns design and operating parameters performance and limitations as well as identifying the potential research avenues in the field.

***Corresponding Author: Nasrul Arahman** (nasrular@usk.ac.id)*

Nafiu Umar Barambu: He is a researcher and academician affiliated with the Department of Chemical Engineering, Syiah Kuala University, Banda Aceh, Indonesia. Nafiu Umar Barambu was a Postdoctoral Research Fellow at the Laboratory of Polymer Science, Department of Chemical Engineering, Faculty of Engineering, Syiah Kuala University, Banda Aceh, Indonesia, from July to December 2024. His research focuses on environmental engineering, water treatment technologies, and membrane-based separation processes, with an emphasis on sustainable engineering solutions.

Nasrul Arahman: He is a professor in the Department of Chemical Engineering, Faculty of Engineering, Syiah Kuala University, Banda Aceh, Indonesia. His research interests include membrane science and technology, water and wastewater treatment, membrane modification, and separation processes. He has published widely in reputable international journals and actively supervises undergraduate and postgraduate research.

Muhammad Roil Bilad: He is an Associate Professor in the Chemical and Process Engineering program, Faculty of Integrated Technologies, Universiti Brunei Darussalam, Brunei. His research interests include polymeric membrane fabrication, membrane fouling, and membrane applications for water and wastewater treatment. He has authored numerous peer-reviewed publications in the field of membrane science and engineering.

Cut Meurah Rosnelly: She is a lecturer and researcher in the Department of Chemical Engineering, Faculty of Engineering, Syiah Kuala University, Banda Aceh, Indonesia. Her research interests include chemical process engineering, environmental technology, and applied chemical engineering. She is actively involved in teaching and academic research.

Sri Mulyati: She is a professor in the Department of Chemical Engineering, Faculty of Engineering, Syiah Kuala University, Banda Aceh, Indonesia. Her expertise lies in membrane processes, water treatment, and separation technology. She has made significant contributions to research, postgraduate supervision, and academic leadership in chemical engineering.

Content

1. Introduction

Membrane separation is a well-established technology widely employed for separation and purification applications in various industries [1–5]. Compared with conventional treatment methods such as adsorption, advanced oxidation, dissolved air flotation, and coagulation–flocculation, membrane-based processes offer superior separation efficiency, higher hydraulic performance, and improved

environmental sustainability [6–9]. Adsorption technology suffers from low separation efficiency for highly concentrated contaminants and generates secondary pollutants from spent adsorbents, making it costly and impractical for large-scale applications [6–12]. Coagulation–flocculation and dissolved air flotation (DAF) are limited by sludge generation, high operational costs, and complex handling requirements [13–17]. Advanced oxidation processes can convert pollutants into less toxic compounds but are often expensive and inefficient for treating large volumes of highly concentrated wastewater [18,19].

Over the past decades, membrane technology has gained increasing attention as a highly efficient and flexible approach for water and wastewater treatment, driven by its ability to deliver consistent performance under diverse operating conditions. In addition, membrane systems typically require a smaller footprint and lower capital and operational costs than many advanced separation technologies, making them attractive for both centralized and decentralized applications [20-24]. Furthermore, membrane processes are characterized by relatively low energy consumption, operational simplicity, and modular design, allowing easy scalability and mobility across different filtration sites [25–29]. However, despite the numerous advantages of membrane technology, the technology is challenged by membrane fouling [30]. Membrane fouling originated from the concentration polarization build-up due to the interaction between the foulant in the feed and the membrane surface [31]. The interplay between the membrane surface and the foulant in the feed invented a boundary layer that consequently deteriorated the overall membrane performance by imposing permeate hydraulic resistance across the membrane [32,33]. The best option to avoid membrane fouling is to control the interaction between the membrane surface and foulant. Thus, the boundary layer formation would be restricted and therefore its impact on the hydraulic resistance would be limited [34,35].

Among several techniques employed for controlling the relationship between the membrane surface and the foulant, feed hydrodynamics is essentially the most economical and eco-friendly approach [36,37]. By imposing feed hydrodynamics, the generated feed turbulent flow exerts higher shear stress on the membrane surface that prevents the foulant interaction with the membrane surface [38], [39]. Higher shear stress is accompanied by higher feed velocity profile and thus the foulant would not have sufficient time to interact with the membrane surface [40]. Moreover, the feed turbulent flow also generated fluid eddies that continuously renewed the concentration polarization and facilitated the back-diffusion of the foulant to the bulk liquid, consequently hindering the foulant interaction with the membrane surface [41-43]. To implement feed hydrodynamics in the membrane filtration system, turbulence promoters and membrane surface patterning are fundamentally the two major techniques as depicted in **Figure 1**.

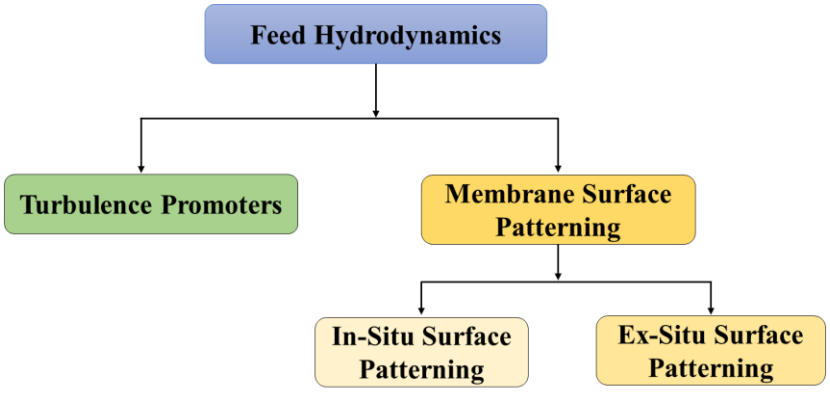

Figure 1. Techniques for imposing feed hydrodynamics

Turbulence promoters are objects placed in a membrane filtration module that induce feed turbulence flow within the filtration system [44,45]. The feed spacer (a polypropylene mesh) is the first turbulence promoter used in membrane filtration systems [46]. Initially, the feed spacer was used to separate between two leaves of membrane in a spiral wound membrane element, but it was realized that it improves the membrane mechanical strength and fluid flow distribution within the membrane effective area [47,48]. Moreover, feed spacers also generate turbulence flow within the filtration cell, which consequently enhances mass transfer by restricting concentration polarization formation [49]. Therefore, these advantages demonstrated by feed spacers encourage rapid development of turbulence promoters and several designs and shapes have been developed, and their applications were expanded beyond spiral wound membrane module [50,51].

Membrane surface patterning is a strategy for generating turbulence flow within the membrane filtration system by imposing patterns topography on the membrane surface [52,53]. The topographical patterns induce secondary flow due to eddies and consequently restrict foulant accumulation on the membrane surface by facilitating the back transport of the foulant to the bulk feed [54,55]. Moreover, membrane surface patterning also increases the membrane effective area due to the extra area provided by the pattern's grooves [56]. In-situ and ex-situ surface patterning are the two major concepts for patterning membrane surfaces. The former involves simultaneous formation of the membrane and its surface patterns at the same time via phase separation micromolding, inkjet printing, or 3D printing, as detailed elsewhere [30,57]. In contrast, *ex situ* surface patterning involves generating patterns on the surface of a ready-made membrane via embossing micromolding [58]. However, despite the advantages posed by turbulence promoters and membrane surface patterning in membrane filtration system, inappropriate designs irritate membrane fouling and thus deteriorate the overall membrane filtration system performance [59,60]. To avoid inappropriate designs of turbulence promoters and membrane surface patterns, many researchers explored computational fluid dynamics (CFD) simulations before the fabrication of the turbulence promoters and membrane surface patterns [61]. Through the CFD simulation concepts, costs, and time can be saved. Moreover, CFD simulation also gives designers freedom to choose the best designs and optimum operating parameters [50, 56].

Therefore, many authors simulated the performance of their turbulence promoters and membrane surface patterns prior to the validation with real filtration systems, this had led to the emergence of many review papers on the application of CFD simulation in membrane filtration systems [50,62,63]. However, almost all the review papers concentrated on the CFD simulation of the turbulence promoter's performance while overlooking that of the membrane surface patterning [64-66]. Therefore, this manuscript aims to fill that gap by reviewing the performance of the CFD simulation of surface patterned membranes and identifying the potential research roadmap in this field.

2. Fundamentals of CFD Simulation for Surface Patterned Membranes

2.1. Governing equations and modeling assumptions

Computational fluid dynamics simulation generally employs a set of numbers that replicate the realistic physical system [67,68]. The set of numbers is normally derived from the governing equation of the real physical system [69,70]. The governing equations are simplified to ease the overall model calculation and minimize error and are presented by Equations 1 and 2.

$$\nabla . u = 0 \quad (1)$$

$$\rho(u . \nabla u) = -\nabla p + \mu \nabla^2 u \quad (2)$$

Where, u is the velocity vector, p denotes pressure (Pa), ρ is the density of water (kg/m^3), and μ denotes dynamic water viscosity (kg/m.s). The simplified form of Newtonian incompressible fluid mass conservation (continuity) equation is presented by Equation 1, while Equation 2 represents the Navier-Stokes (momentum conservation) equation [71,72]. The governing equations are integrated using the SIMPLE algorithm (acronyms for Semi-Implicit Method for Pressure Linked Equations) and the k-ε model [73-75]. The segregated model domains are solved using the finite element method (FEM).

2.2. Boundary conditions and key hydrodynamic parameters

To simplify the calculation, the model domains are assumed to be fixed and impermeable, while flow is assumed to be fully developed across the domains and solid walls are imposed with no-slip boundary conditions.
COMSOL Multiphysics and Ansys Fluent are widely adopted CFD simulation software by most authors because of their user-friendly advantages and incorporation of the design and development tools in their simulation domain [75,76]. For surface-patterned membranes, the main simulation element in the CFD model is "Surface Shear Stress". The larger the surface shear stresses, the lesser the concentration polarization build-up and consequently the greater the mass transfer coefficient [77]. Essentially, large shear stress is always accompanied by a higher velocity profile within the system, which consequently restricts the interplay between the membrane surface and foulant particles since the foulant particles do not have enough time to interact well with the membrane surface.

3. Hydrodynamic Performance of Surface Patterned Membranes: CFD Insights

3.1. Shear stress distribution and flow behavior over patterned membranes

Mazinani *et al.* [78] explored ex-situ surface patterning techniques to pattern the surface of a polyethersulfone (PES) membranes. They deposited a flat PES membrane onto a wavy porous 3D printed support using vacuum filtration. The flat PES membrane replicated the wavy patterns of the 3D printed support and thus the surface of the membrane became patterned. By simulating the hydrodynamic performance of the wavy and the flat PES membrane using COMSOL Multiphysics software, the flat membrane showed uniform shear stress distribution of 0.26 Pa across its surface. In contrast, the patterned membrane recorded a heterogeneous shear stress across its surface with 1.43 Pa as the highest shear stress exerted (at the pattern peaks) while operating at the Reynolds number (Re) of 1000.
For surface-patterned membrane channels, the Reynolds number is defined using Equation 3:

$$Re = \frac{\rho.U.D_h}{\mu} \quad (3)$$

Where, ρ is the fluid density (kg.m^{-3}), U is the bulk or superficial feed velocity (m.s^{-1}), μ is the dynamic viscosity (Pa·s), and D_h is the hydraulic diameter of the patterned channel. The hydraulic diameter is calculated based on the effective flow cross-section, accounting for surface patterns, and is given by $D_h = 4A/P$, where A is the flow area and P is the wetted perimeter including pattern peaks and valleys.

3.2. Effect of operating conditions on hydrodynamic performance

The imbalance in the shear stress demonstrated by the wavy membrane is due to the flow instability posed by the wavy patterns. The flow instability generated fluid eddies that continuously swept away the foulant from the membrane surface and thus encouraged the back-diffusion of the foulant to the bulk fluid, thereby restricting boundary layer formation and thus limiting its impact on the membrane hydraulic performance [78].
The impact of the wavy patterns on the membrane surface shear stress became more prominent by operating at higher Reynolds

number. At Re of 1400, the shear stress at the peak of the wavy membrane reached up to 2.12 Pa while the flat membrane demonstrated 0.34 Pa shear stress across its surface. By validating the CFD simulation result with 1 g/L fouling solution of bovine serum albumin (BSA) at 1 bar transmembrane pressure, the wavy membrane sustained up to ~ 85% of its initial permeance whereas its flat counterpart retained just 36% of its initial permeance. This justifies the linear proportionality between the membrane surface shear stress and surface fouling resistance. The impact of shear stress on the antifouling performance of the membrane became more pronounced by adjusting the Reynolds number from 1,000 to 1,400 (a 40% increase). The surface shear stress of the flat membrane surged by 30.8% (from 0.26 to 0.34 Pa) while that of the wavy membrane increased by up to 48.3% (from 1.43 to 2.12 Pa). Therefore, the impact of surface patterned membrane on fouling resistance became more effective by operating at high Reynolds number [78].

3.3. Identification of fouling-prone regions

Recently, Barambu *et al.* [75] patterned the surface of polysulfone (PSF) membrane via a novel concept of patterning the filtration module. By depositing the flat PSF membrane on the patterned channel, the membrane mimicked the wavy patterns of the channel on its surface. The authors examined four different locations of the wavy membrane and extracted their respective shear stresses. The examined locations are the pattern valley (A), just after the valley (B), the pattern peak (C) and just after the peak (D) as depicted in **Figure 2**. The flat membrane recorded a homogeneous shear stress of 0.17 Pa throughout its surface while the wavy patterned membrane exerted 0.596 Pa at the wavy peak (C). At points B, D, and A, the shear stress absorbed recorded were ~ 0.39 Pa, ~ 0.23 Pa and 0.18 Pa, respectively. The patterned membrane recorded up to ~ 6% improved shear stress even at the lowest shear stress location (wavy valley (A)) compared to the shear stress recorded by the flat membrane (0.17 Pa). Point B and D exerted an enhanced shear stresses of up to 132 and 31%, respectively, compared to the baseline flat membrane. The validation results aligned with the CFD results; the wavy membrane recorded improvement in the hydraulic output of up to ~ 58% even after 11.7 hours of fouling filtration compared to the pristine flat membrane. This was due to the hydrodynamic effect induced by the wavy surface patterns, which accounted for up to ~ 58% improved membrane lifespan. Moreover, by evaluating the impact of the wavy patterns on the membrane packing density, 18% of the enhanced hydraulic output is attributed to the increased effective membrane area while the remaining 40% is attributed to hydrodynamic impact of the wavy patterns [75]. Shang *et al.* [79] also reported an improved shear stress at the ridge valley of a micro-patterned nanofiltration membrane as compared to the flat baseline nanofiltration membrane. The patterned membrane recorded a shear stress of 9.7 Pa, while the flat membrane recorded just 1.9 Pa under the same operating crossflow velocity of 10 cm/s.

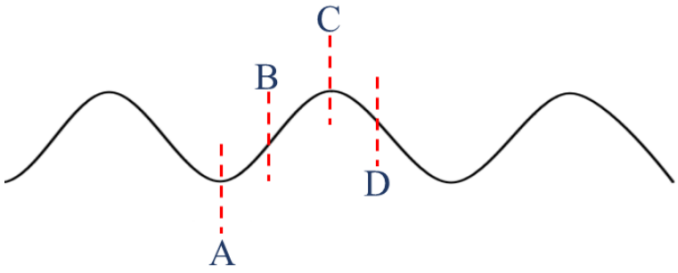

Figure 2. Examined locations of the wavy patterned membrane

However, by adjusting the crossflow velocity from 10 to 100 cm/s, the impact of the surface patterned membrane on the shear stress became evident. The surface of the patterned membrane absorbed up to 190.1 Pa shear stress compared to 26.6 Pa recorded by its flat counterpart. Hence, this result further confirms that the impact of surface patterned membranes on fouling resistance became significant by operating at high operating parameters (crossflow velocity).

Similarly, Jung *et al.* [80] also recorded the highest shear stress at the apex of the surface patterned membrane and the lowest shear stress at the valleys of the patterns. **Figure 3** illustrates the names given by various authors for the highest and the lowest shear stress positions. Since the upper region of any kind of pattern design demonstrated the highest shear stress, it is expected to have a substantial influence on the renewal of the boundary layer and consequently restrict foulant interaction with the membrane surface. In contrast, in the lower region, where the shear stress exerted is less, foulant has better change to reside and form concentration polarization that encourages membrane fouling formation. Therefore, under these conditions, at low crossflow velocity, the flat membrane recorded a higher surface shear stress of 1 Pa compared to 0.6 Pa demonstrated by the lower region of the surface patterns. However, the upper region of the surface patterns exerted up to 3.7 Pa shear stress [81]. Therefore, under this condition, the lower region of the patterned membrane will be fouled prior to the flat membrane, while the upper region of the patterned membrane has up to 270% enhanced lifespan compared to the flat membrane. Similarly, Shang *et al.* [82] also recorded the highest wall shear stress at the hills of micro-sized patterns of a nano filtration membrane, as well as vortices around the bottom region of the patterns. The patterned membrane demonstrated an enhanced fouling resistance performance, indicated by its higher hydraulic output and least mass transfer decline compared to the baseline flat membrane. The control nano filtration membrane exerted surface shear stress of 0.02 Pa while the micro-patterned nano filtration membrane recorded 0.3 Pa shear stress at its pattern peak. This result revealed that the patterned membrane significantly prevents fouling formation by scouring the foulant from membrane surface by up to 15-fold compared to the control flat membrane. The patterned membrane recorded a normalized flux of 0.8 compared to 0.48 demonstrated by the flat membrane after 20 hours of 2 g/L silica nanoparticle fouling filtration. The patterned membrane also recorded an enhanced normalized flux of up to 20% (from 0.8 to 0.96) by raising the operating parameter from 30 to 50 cm/s [82].

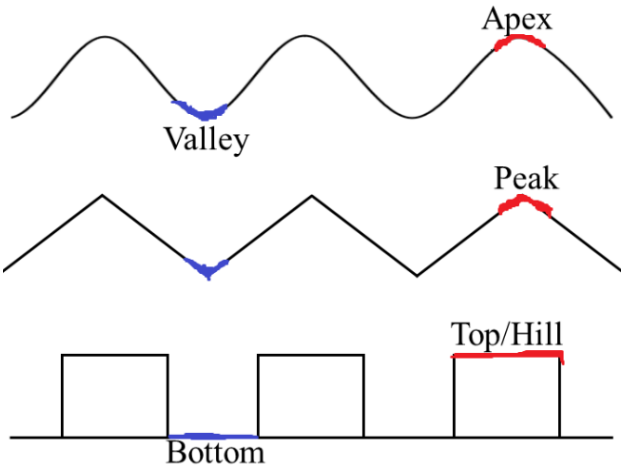

Figure 3. Demonstration of the highest (Red) and lowest (Blue) shear stress position within the patterns

Therefore, this result justifies the influence of the operating parameter (crossflow velocity) on the antifouling performance of surface patterned membranes.

The flow direction of the feed to the patterns of the surface patterned membrane was also reported to have intensive impact on the antifouling performance of the membrane. The fouling resistance performance of flow directions, parallel, perpendicular and angular to the patterns of the patterned membrane were examined, and the perpendicular flow direction demonstrated an outstanding antifouling performance. By flowing 50 ppm activated sludge perpendicular to the patterns of the patterned membrane, the membrane recorded water flux of 105.51±1.39 $m^3/m^2.d$. While adjusting the feed flow direction to parallel and angular to the patterns, the water flux declined to 103.30 ± 1.36 and 102.64±1.44 $m^3/m^2.d$, respectively. The flat membrane recorded hydraulic resistance of 9.61E+10 m^{-1} and water flux of 90.27 ± 1.27 $m^3/m^2.d$, it resulted in 14.4% decline in the membrane life cycle as compared to the patterned membrane with perpendicular flow orientation [83]. Therefore, to harness the ultimate potential of surface patterned membrane for membrane fouling management, operating parameters as well as the flow direction must be optimized. Despite their usefulness, CFD studies of membrane systems often rely on simplifying assumptions that limit their predictive accuracy. Many models assume Newtonian fluid behavior, thus neglecting the non-Newtonian rheology commonly associated with concentrated feeds, biofilms, and particle-laden suspensions. To reduce computational cost, two-dimensional (2D) simulations are frequently employed, which may fail to capture three-dimensional flow structures, secondary vortices, and spatial heterogeneities that are critical to mass transfer and fouling development. Moreover, most CFD investigations emphasize short-term hydrodynamics and represent fouling using static or simplified boundary conditions, thus overlooking long-term fouling evolution, membrane aging, and dynamic foulant–membrane interactions under realistic operating conditions.

4. Effect of Surface Pattern Design Parameters on Antifouling Performance

4.1. Influence of pattern geometry

Ilya *et al.* [59] examined the influence of pattern design, dimensions, and pattern gaps on the hydrodynamic performance of the surface patterned membrane. Moreover, the wall shear stress of three sections (top, middle, and bottom) of each pattern design was also studied. The details of the geometries are presented in **Table 1**.

4.2. Effect of pattern dimensions and spacing

Pattern dimensions and spacing play a decisive role in governing the hydrodynamic response of surface-patterned membranes, as they directly control the intensity and distribution of flow disturbances near the membrane surface. CFD studies consistently show that increasing pattern height or depth enhances local shear stress and promotes vortex formation, thereby improving foulant removal. However, irrationally large features generated a stagnation zone within pattern valleys and thus increased the flow resistance. Similarly, pattern spacing determines the interaction between the adjacent flow disturbances, a closely spaced patterns can intensify shear but risk hydraulic shielding, while widely spaced patterns diminish hydrodynamic effectiveness. These findings highlight the necessity of optimizing pattern dimensions and spacing so as to balance the shear enhancement, fouling mitigation, and pressure-drop penalties. The flat membrane demonstrated a uniform local wall shear stress of 0.21 Pa while the patterned membrane exhibited heterogeneous wall shear stress depending on the position and pattern design as shown in **Table 2**.

Table 1. Details of the membrane pattern geometry

Membrane code	a	b	c	Geometry design
	(μm)			
R500	500	500	500	Rectange 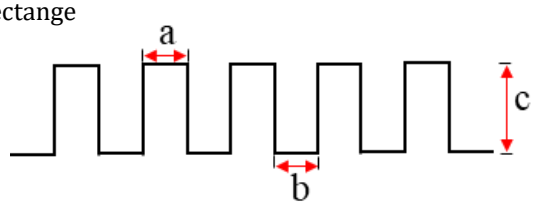
R1000	500	500	1000	
R1500	500	500	1500	
C500	500	500	500	Circle 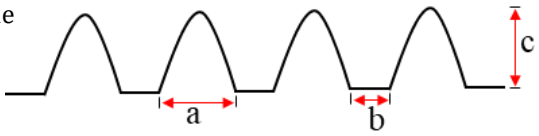
T100	500	0	500	Triangle 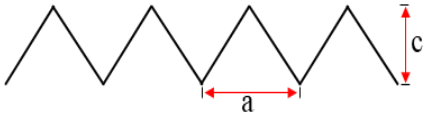

a: Pattern width, b: Pattern Gap, and c: Pattern height

Table 2. Wall shear stress exerted at various locations of surface patterned membrane

Membrane code	Wall shear stress (Pa)			
	Bottom of the patterns	Middle of the patterns	Top of the patterns	Total
R500	0.21	0.67	3.9	4.78
R1000	1.08	1.58	0.42	3.08
R1500	1.3	2.67	1.75	5.72
C500	0.07	0.67	1.58	2.32
T100	0.07	1.01	3.67	4.75

R1000 and R1500 membranes recorded highest shear stress at the bottom (valley) of their patterns by absorbing up to 1.08 and 1.3 Pa respectively. These results illustrate the significance of the fluid eddies generated by R1000 and R1500 membranes in facilitating the back-diffusion of the foulant to the bulk fluid and thus disrupting the boundary layer formation and posed the membrane with antifouling property. Unlike R500 membrane that does not generate fluid eddies at its valley and exerted same wall shear stress as the flat membrane (0.21 Pa). While C500 and T100 membrane recorded a worse scenario of allowing the foulant to reside at their pattern valley and initiated membrane fouling. They both recorded a very low shear stress of just 0.07 Pa at their pattern's valleys [59]. R1000 and R1500 also outperformed other membranes by absorbing 1.58 and 2.67 wall shear stress at the middle of their patterns. However, T100 recorded up to ~ 51% enhanced wall shear stress exerted at the middle of its patterns compared to that of the R500 and C500 membranes. While at the top/apex of the patterns, T100 and R500 demonstrated the highest shear stress by

recording up to 3.67 and 3.9 Pa respectively. However, considering the overall wall shear stress absorbed by each membrane, R1500 recorded the highest with up to 5.72 Pa shear stress followed by R500 and T100 with total wall shear stress of 4.78 and 4.75 Pa respectively [59]. Despite the high overall shear stress demonstrated by R500 and T100 membrane, they both allow foulant to reside at their pattern's valleys thereby encouraging membrane fouling formation. Therefore, pattern design optimization is required via CFD simulation to obtain the best fouling resistance design. Based on the results of the shear stress absorbed by the membranes (**Table 2**), R1500 demonstrated the highest fouling resistance ability followed by R1000 and R500 respectively. This is because the membranes exerted adequate shear stress and generated swirling effect that drives away the foulant from the membrane surface across all its surface regardless of the position. In the case of T100, the membrane absorbed good overall shear stress but with very poor shear stress at the valleys of its patterns and thus motivate fouling formation at the valleys of the membrane [59]. Therefore, overall shear stress is not only the deciding factor but also the shear stress absorbed at various locations of the surface patterned membrane. Similarly, Choi *et al.* [84] also reported similar trends after examining the effect of unit and pattern spacing in a reverse osmosis membrane. The patterned membrane with unit and pattern spacing of 2 µm elucidated the best antifouling performance by maintaining normalized flux of up to 0.8. While by using 6 µm as unit and pattern spacing, the membrane recorded normalized flux of 0.66 and 0.53, respectively.

Lower overall shear stress can still result in better antifouling because fouling is governed by local hydrodynamics and particle trajectories, not average shear alone. Localized shear peaks, vortices, and secondary flows can periodically lift particles from the membrane surface, reduce residence time, and disrupt attachment even when mean shear is low. In contrast, high, uniform shear may continuously drive particles toward the membrane, compress foulant layers, and promote irreversible deposition. Thus, effective vortex dynamics and flow-induced particle migration often provide superior antifouling performance compared to simply increasing overall shear stress.

5. Influence of Foulant Characteristics and Operating Conditions

5.1. Effect of foulant size and physicochemical properties

Similarly, membrane fouling resistance performance also depends on the size of the foulant particle as depicted in **Figure 4**. Therefore, it is important to optimize the pattern geometry in relation to the foulant particle size and operating parameter for an enhanced membrane fouling resistance. The FM, nano-patterned membrane (NPM) and micro-patterned membrane (MPM) demonstrated heterogeneous fouling resistance performance depending on the foulant particle size. During validation of the CFD result with a real experimental study, four model fouling feeds with foulant diameters of 0.1, 0.5, 2, and 6 µm were used to investigate the influence of the foulant size on the fouling resistance performance of the surface patterned membranes [85]. During 0.1 µm foulant size fouling filtration, the patterned membranes (NPM and MPM) recorded an enhanced fouling resistance compared to the flat membrane. The mass of the foulant deposited on the flat membrane is up to 36.6 mg/m^2 while NPM and MPM recorded 34.2 and 30.8 mg/m^2, respectively. By adjusting the foulant size to 0.5 µm, the antifouling performance of MPM membrane deteriorated, while that of the NMP membrane became notable. The MPM membrane fouling resistance is just slightly beyond that of the flat membrane, up to 38.3 mg/m^2 of the foulant deposited on the MPM membrane whereas the flat membrane adsorbed 40.0 mg/m^2. Comparatively, the NMP membrane demonstrated up to 46.5% and 44.1% enhanced antifouling performance as compared to FM and MPM membrane, respectively.

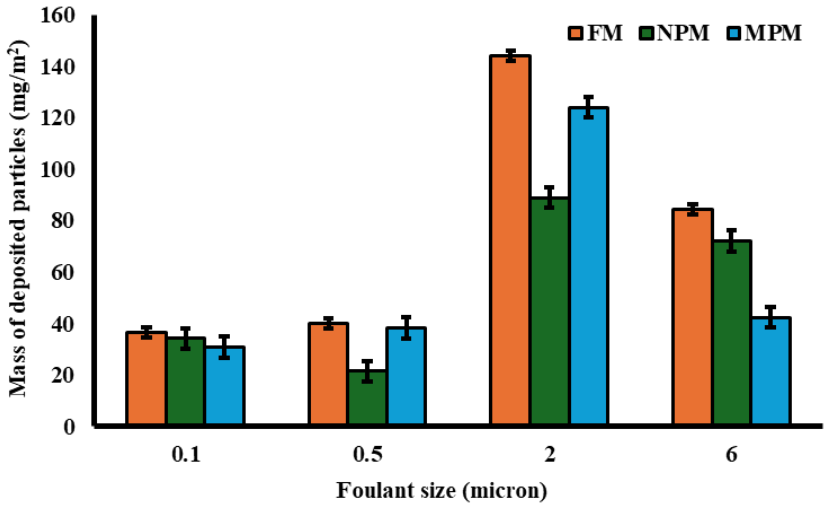

Figure 4. Performance of the membranes during aqueous suspension of polystyrene latex microspheres fouling filtration with different foulant sizes

The micro-patterned membrane regained its outstanding antifouling performance during 6 µm feed fouling filtration; the membrane recorded up to 49.64% and 41.1% enhanced fouling resistance performance compared to FM and nano-patterned membranes, respectively. The NPM membrane also recorded about 14.5% improved fouling resistance compared to the baseline FM membrane. Therefore, the instability in the fouling resistance performance of the membranes with regard to the foulant size justifies the need for foulant size consideration during pattern design of the surface patterned membranes for an optimum fouling resistance performance.

5.2. Interaction between foulant characteristics and pattern scale

Similar trends were also reported by Lin *et al.* [86]. The millimeter-scale (PM60), micro-scale (PM55), and nano-scale (PM50) microfiltration membranes exhibited shear stress of 0.3978, 0.0302, and 0.0305 Pa, respectively. The performance of the membranes for resisting 2 g/L diatomaceous earth solution deposition revealed PM55 as the best-performing membrane in terms of fouling resistance. The PM55 membrane recorded foulant deposition of 191.6 mg/m^2 against 241.6, 271, and 276 mg/m^2 exhibited by PM50, PM60, and the flat membrane, respectively. This result further disclosed the influence of foulant characteristics on membrane antifouling performance despite the magnitude of the shear stress absorbed by the membrane surface. PM60 exerted highest shear stress but PM55 demonstrated the best antifouling performance despite its less surface shear stress compared to PM60 membrane. This is due to the foulant particle characteristic as reported by Jang *et al.* [85] and described in **Figure 4**.

Zhou *et al.* [87] patterned the surface of a reverse osmosis membrane, and the validation result corresponded with the CFD simulation result. The simulation result indicated the great influence of the surface patterns on the velocity and wall shear stress of the filtration system. The peaks of the patterns show the highest velocity and the wall shear stress, while the valleys recorded lower velocity as well as the wall shear stress. However, some vortices were observed in the valley despite the low velocity profile recorded. Although the vortices do not have any impact on the fouling resistance performance since the swirling force generated by the vortices is weak to drive the foulant away from the membrane surface, but they rather encourage foulant settlement in the valley. The concentration polarization at the valley of the patterned membranes is up to 64% higher than

the baseline flat membrane. However, despite the higher fouling propensity recorded at the valleys of the patterns, the patterned membrane recorded up to 40% enhanced nominal permeate flux compared to the baseline flat membrane attributed to the enhanced packing density created by the grooves of the surface patterns [87]. The surface patterns of the membranes created an additional effective membrane area for more hydraulic output due to the extra space provided by the pattern grooves, which in turn enhances the membrane packing density.

5.3. CFD-guided optimization under different operating conditions

Liu *et al.* [88] developed a novel innovation for generating turbulent flow within the membrane filtration system. They fabricated saw-tooth patterns on the upper/top channel of the filtration cell, while the lower/bottom channel remained flat and housed the membrane. The top patterned channel generated hydrodynamic effect on the membrane surface with shear rate of up to 6400 L/s while the flat module recorded just 2200 L/s. The validation results confirmed the simulation performance of the patterned membrane. The patterned setup achieved a steady state flux of 1.75×10^{-4} m/s while treating 10 µm polystyrene particles suspension at 60 kPa transmembrane pressure whereas its flat counterpart recorded 5.1×10^{-5} m/s. This result confirmed the effect of the vortices generated by the patterns of the upper channel that impacted the membrane in the lower channel. The vortices intensified fluid mixing and thus favored the back diffusion of the foulant to the bulk fluid, thereby limiting boundary layer formation and consequently limited its influence on the mass transfer performance of the membrane.

The antifouling performance of the patterned membrane filtration system became noticeable by raising the transmembrane pressure from 60 kPa to 100 kPa. The patterned filtration setup recorded 250% enhanced antifouling performance by sustaining a steady state flux of 2.1×10^{-4} m/s against 6.0×10^{-5} m/s demonstrated by the flat filtration setup [88]. This result further justifies that by employing an appropriate pattern design and filtration system operating parameters, the impact of hydrodynamics and membrane packaging density can be harnessed, and the optimum antifouling performance of the surface patterned membranes can be achieved. So far, the fouling resistance performance of surface patterned membranes is well established, and the real experimental results always align with the simulation output as per as all necessary parameters are considered. **Table 3** presents the antifouling performance of the surface patterned membranes.

6. Influence of Membrane Surface Patterning on the Filtration System Energy Consumption

It has been traditionally believed that surface patterned membranes consume higher energy as compared to their flat counterpart membranes due to pressure drop initiated by their surface patterns. However, by evaluating and comparing the overall energy consumption of the surface patterned membrane setup and that of the flat membrane setup, energy savings of up to 21% were reported despite the pressure drops of 7% generated by the membrane surface patterns. The flat membrane setup consumed 0.019 kWh/m^3 while the patterned membrane setup under the same operating condition consumed 0.015 kWh/m^3 [75]. Similarly, the flat membrane setup required 0.022 kWh/m^3 for its operation against 0.016 kWh/m^3 demanded by its patterned counterpart setup. Thus, recording up to 28% energy savings by just introducing fouling mitigation mechanism via feed flow turbulence generation [89]. Moreover, other membrane fouling mitigation techniques also recorded tremendous energy saving. Improving additive density within the membrane matrix via membrane surface chemistry development recorded up to 66% energy saving. The baseline membrane exhibited energy consumption of 0.08 kWh/m^3 against 0.027 kWh/m^3 consumed by the antifouling membrane [90]. Feed flow turbulence generation demonstrated a

significant energy saving despite the pressure drop. The energy saving overwhelmed the effect of the pressure drop and consequently manifested the economic advantage of the feed turbulence flow [33,75,89]. The energy saving performance of feed turbulence depends of the turbulence generating technique employed. By employing static mixer as turbulence generator, 40% energy saving was recorded [91] while by applying rotating disks with vanes reported 58% energy saving were [92]. Therefore, the energy-saving performance of feed turbulence flow generation techniques has been established and gained industrial adoption.

7. Correlation between CFD Predictions and Experimental Validation

To establish the credibility and practical applicability of CFD approaches in the context of surface-patterned membranes, it is important to juxtapose simulation results with empirical observations. Several investigations have pursued such CFD–experiment comparisons to evaluate how well flow predictions, fouling behavior, and performance trends manifest under actual operating conditions. **Table 3** compiles key studies that systematically link CFD outcomes with experimental validation, highlighting agreements, limitations, and areas where predictive modeling requires further refinement.

Table 3. Summary of simulation and validation fouling resistance performance of surface patterned membranes

Simulation result	Operating parameters	Validation result and findings	Ref.
Shear stress at Re = 1000: Flat membrane = 0.26 Pa Patterned membrane = 1.43 Pa Shear stress at Re = 1400: Flat membrane = 0.34 Pa Patterned membrane = 2.12 Pa	Feed: 1 g/L BSA solution TMP: 1 bar Re: 1000-1400	Hydraulic performance: Flat membrane = sustained 36% of its performance after BSA fouling filtration Patterned membrane = retained 85% of its hydraulic performance after BSA fouling filtration CFD simulation results represent the real system and the results are aligned. Performance of surface patterned membrane became bold by operating at higher Re.	[93]
Surface shear stress: Flat membrane = 0.17 Pa Wavy-patterned membrane = 0.596, 0.39, 0.23 and 0.18 Pa at the wavy peak, just before the peak, just after the peak and at the valley, respectively	Feed: 1000 ppm oil/water emulsion TMP: 0.2 bar	The wavy patterned membrane recorded hydraulic output of up to 58% improvement compared to its pristine flat membrane By fixing appropriate design specifications and operating parameters, the valley of the wavy membrane recorded up to 6% enhanced shear stress compared to the flat control membrane.	[75]

Simulation result	Operating parameters	Validation result and findings	Ref.
Shear stress at CFV = 10 cm/s: Flat membrane = 1.9 Pa Patterned membrane = 9.7 Pa Shear stress at CFV = 100 cm/s: Flat membrane = 26.6 Pa Patterned membrane = 190.1 Pa	Feed: 2 g/L colloid silica CFV: 10 and 100 cm/s	Fouling resistance performance of surface patterned membranes became bold by operating at higher CFV	[79]
Surface shear stress (Pa): Flat membrane = 0.02 Patterned membrane = 0.3	Feed: 2 g/L silica nanoparticle CFV: 30 and 50 cm/s	The patterned membrane also recorded an enhanced normalized flux of up to 15-fold compared to the flat membrane. By raising the operating parameter from 30 to 50 cm/s, the hydraulic output of the patterned improves by 20% Fouling resistance performance of surface patterned membranes depends on the operating parameter (CFV) employed.	[82]
The surface patterns of the patterned membrane exerted higher shear stress by feeding the feeds perpendicular to the patterns compared to that of parallel and angular.	Feed: 50 ppm activated sludge. TMP: 50 kPa	Normalized flux: Perpendicular setup = 0.31 Parallel and angular setup = 0.29 Flat membrane = 0.2. Feeding the feed perpendicular to the patterns of the surface patterned membrane remains the best option to harness the optimum fouling resistance performance of surface patterned membranes.	[83]
Surface shear stress (Pa): Rectangular patterns setup = 5.72 Circular patterns setup = 2.32 Triangular patterns setup = 4.75	Feed: 1 g/L BSA solution	Rectangular patterns setup showed less BSA adsorption and higher permeance compared to the flat membrane and other patterns setup The rectangular pattern setup recorded optimum fouling resistance performance than circular and triangular pattern setup. Thus, rectangular pattern setup is the optimum design based on the operation parameters employed than circular and triangular setup	[59]

Simulation result	Operating parameters	Validation result and findings	Ref.
Surface shear stress: 2-Micron pattern spacing setup recorded highest shear stress compared to 6-micron pattern spacing	Feed: 103 CFU/mL *P. aeruginosa* solution	Normalized flux: 2-Micron pattern spacing = 0.8 6-Micron pattern spacing = 0.53 Pattern and unit spacing has significant influence on the antifouling performance of surface patterned membranes	[84]
Surface shear stress (Pa): PM60 patterned membrane = 0.398 PM55 patterned membrane = 0.030 PM50 patterned membrane = 0.031	Feed: 2 g/L diatomaceous earth solution	Surface foulant deposition ($mg/m^{2)}$: PM55 = 191.6 PM50 = 241.6 PM60 = 271 Flat membrane = 276 Fouling resistance of surface patterned membranes depends on the pattern design specifications	[86]
Shear rate (l/s): Flat module = 2200 Patterned module = 6400	Feed: 10 µm polystyrene particles suspension TMP: 60 kPa	Steady state flux (MS): Patterned module = 1.75×10^{-4} Flat module = 5.1×10^{-5} Patterned membrane recorded an enhanced resistance of particle deposition on its surface compared to the flat membrane	[88]
Surface shear stress (Pa): Circular pattern setup = 3.37 Kite pattern setup = 4.38 Tear drop pattern setup = 4.63 4-tipped star pattern setup = 4.37	Feed: 10 mg/L Polystyrene particles solution Feed flow rate = 1.667 g/s CFV = 0.104 m/s	Recirculation zones were observed in 4-tipped star patterns and circular pattern setup while kite patterns and tear drop patterns exhibited continuous flow and reconnection of the streamline just after the patterns. The recirculation zones of 4-tipped star patterns and circular pattern setup encourage particles deposition on the membrane surface.	[94]

Simulation result	Operating parameters	Validation result and findings	Ref.
Surface shear stress (N/m^2): Patterned membrane: Pattern apex: 3.7 Pattern valley: 0.6	Feed: 10 ppm poly (methyl methacrylate) colloidal suspension (diameter=1.3 μm)	The pattern of the surface patterned membrane was divided into four sections and their respective particles depositions were extracted as follows: Apex front = 5.05 × 10−2 μm^{-2} Apex back = 4.64 × 10−4 μm^{-2} Valley front = 0.494 μm^{-2} Valley back = 0.372 μm^{-2} The valley region of surface patterned membranes is the fouling initiating region with valley front as the highest fouling region followed by valley back and apex back.	[80]
The introduction of intervals between the patterns increases the vortex formation in the valley of the surface patterned membrane	Feed: 2 μm latex particle suspension CFV = 0.4 m/s	Mass of particle deposition on the membrane surface (mg): Patterned membrane with pattern spacing = 10.8 Patterned membrane without pattern spacing = 44.5 Flat membrane = 75.3 Introducing intervals between patterns of surface patterned membrane enhances its antifouling performance.	[95, 96]
Shear stress (Pa): Flat membrane = 5.27 Line patterns membrane = 5.93 D-line patterns membrane = 6.11 Sharklet RC membrane = 6.32 Sharklet AF membrane = 16.0	Feed: 103 CFU (colony forming units) mL^{-1} Operating pressure: 15.5 bar	Surface biofilm density ($\mu m^3/\mu m^2$): Flat membrane = 4.9 ± 0.9 Line patterned membrane = 2.8±0.6 D-line patterned membrane = 1.9±1.0 Sharklet RC = 1.2±0.7 Sharklet AF membrane = 0.4±0.2 Sharklet AF patterned membrane generated an enhanced secondary flow that restricted biofilm formation on its surface compared to flat and other patterned designs setups.	[97]

8. Performance of Surface Patterned Membranes in Various Membrane Processes

The enhanced performance recorded by surface patterned membranes compared to the traditional flat membranes has been extended beyond pressure driven membrane filtration systems [98-100] and wastewater treatment [101]. Chang *et al.* [102] explored membrane surface patterning to improve the overall performance of membrane photothermal filtration systems. The surface of carbon black/polyacrylonitrile membrane was embossed via thermal imprinting. The patterned membrane recorded an enhanced clean water evaporation rate and thermal conversion efficiency of 1.33 kg m^{-2} h^{-1} and 86% respectively. The performance of the patterned membrane accounted for approximately 5% and ~ 4% for water evaporation rate and thermal conversion efficiency, respectively, compared to the baseline flat membrane. This result grants motivation to explore the optimum potential of membrane surface patterning in a thermally driven membrane filtration system.

Global interest in green energy production (hydrogen) is on the rise due to continuous environmental calamities caused by global warming due to the release of carbon dioxide by traditional fossil fuels. Recently, by imposing rough patterns on the surface of the membrane utilized in the electrolysis setup, up to 26% improvement in hydrogen production was recorded. The patterned membrane produced 0.767 g of hydrogen and efficiency of 20.67 g.H_2/kWh while the pristine flat membrane generated 0.608 g hydrogen with efficiency of 20.47 g.H_2/kWh [103]. The potential of surface patterned membrane in enhancing the overall performance of Alkaline membrane electrolyzers was also explored by Hu *et al.* [104] and up to 39 and 23% improvement in water permeability and electrochemical surface area were recorded compared to flat membrane with the same catalyst loading. Therefore, these results attested to the performance of the surface patterned membranes in enhancing green energy production and vested the opportunity for further exploration.

Despite the growing body of CFD studies on surface-patterned membranes, several clear trends, contradictions, and knowledge gaps emerge from the literature. A consistent trend is the enhancement of wall shear stress and vortex intensity with increasing Reynolds number and pattern depth; however, reported performance gains vary widely due to differences in pattern geometry, channel definition, and evaluation metrics. Contradictory findings are observed regarding optimal pattern dimensions, where some studies report improved antifouling performance with deeper valleys, while others indicate increased pressure drop and localized fouling at excessive pattern heights. Moreover, most CFD investigations assume mono-dispersed foulants and steady-state flow conditions, overlooking the coupled effects of foulant size distribution, deformability, and transient flow behavior. These gaps highlight the need for standardized hydrodynamic performance metrics, multi-scale fouling models, and systematic CFD–experimental validation to enable more reliable design guidelines for surface-patterned membrane systems.

9. Conclusion and Future Perspectives

Computational fluid dynamics simulation has the potential to represent and simulate the real membrane filtration system to obtain optimum design specifications and best operating parameters as discussed in this review manuscript. Moreover, this manuscript also provides details on the establishment of membrane surface patterning as a non-chemical and facile approach for membrane fouling management. However, despite the fouling management performance demonstrated by the surface patterned membranes and the CFD simulation potential to represent the real membrane system, some parameters such as operating parameters (*e.g.,* crossflow velocity, Reynolds number, etc.), foulant size and flow direction, must be considered while designing the surface pattern to achieve the optimum design for membrane fouling resistance. By operating at an optimized operating parameters,

efficient vortices would be generated even at the pattern valleys (lowest shear stress location) that swept and encourages the diffusion of the foulant to the bulk fluid. Therefore, for any set of pattern design specifications (pattern height, width, spacing, etc.), an optimized operating parameter must be obtained during CFD simulation step. While pattern design specifications relied on the foulant size. Therefore, there is inter correlation between pattern design specifications, operating parameters and foulant size. Thus, their inter correlation necessitates the use of CFD simulation to obtain the best combination that exploited the full potential of membrane surface patterning for membrane fouling resistance. Apart from the hydrodynamic effects induced by the surface patterns of patterned membranes for fouling resistance, the surface patterns also boost the membrane hydraulic output by providing additional available membrane effective area originating from the pattern hill for hydraulic permeation. The provision of an additional membrane effective area, inaugurated by the surface patterned membranes extended its application from pressure driven membrane filtration systems to other non-pressure-driven membrane filtration systems (such as concentration and thermal driven, etc.), as well as other membrane separation systems. Therefore, there is an intensive need to explore membrane surface patterning design specifications to improve its packaging density performance and to design a pattern valley that would generate efficient vortices even at lower operating parameters. Through this, membrane surface patterning would revolutionize filtration and separation processes. Recent advances in data-driven approaches offer new opportunities to complement CFD-based membrane design. The integration of machine learning and optimization algorithms with CFD simulations can facilitate multi-parameter optimization by efficiently exploring large design spaces involving geometric features, operating conditions, and material properties. In parallel, the development of adaptive or smart flow-channel patterns, whose geometry or surface properties respond to hydrodynamic or fouling conditions, represents a promising direction for enhancing antifouling performance while maintaining energy efficiency. Although these approaches remain at an early stage of development, they highlight the potential of combining physics-based CFD models with data-driven tools to accelerate rational membrane and pattern design.

Acknowledgment

The authors would like to acknowledge Universitas Syiah Kuala for the financial support of this work through the PDRA research grant (487/UN11/SPK/PNBP/2024). They would also like to gratefully acknowledge the Indonesian Endowment Fund for Education (LPDP), under the Ministry of Higher Education, Science, and Technology, through the EQUITY Program (Contract No. 4318/B3/DT.03.08/2025 and No. 491/UN11/HK.02.06/2025), for supporting the article processing charge (APC) of this publication.

Conflicts of Interest

The authors declared no conflict of interest.

Authors' Contribution

The authors contributed equally to this manuscript: Nafiu Umar Barambu: Writing original draft, review and editing, Project administration and investigation. Nasrul Arahman: Writing, review and editing, project administration and funding acquisition. Mohammad Roil Bilad: Writing, review and editing, project administration. Sri Mulyati: Writing, review and editing, Project administration. Cut Meurah Rosnelly: Writing, review and editing, project administration.

ORCID

Nafiu Umar Barambu
https://orcid.org/0000-0001-5641-1317

Sri Mulyati
https://orcid.org/0000-0001-5865-4769

Cut Meurah Rosnelly
https://orcid.org/0000-0003-0531-3674

Mohammad Roil Bilad
https://orcid.org/0000-0001-7292-6046

Nasrul Arahman
https://orcid.org/0000-0001-5077-2867

References

[1] Ibrahim, Y., Hilal, N. Enhancing ultrafiltration membrane permeability and antifouling performance through surface patterning with features resembling feed spacers. *NPJ Clean Water*, **2023**, 6(1), 60.
[2] Rahman, N.A., Sotani, T., Matsuyama, H. Effect of the addition of the surfactant tetronic 1307 on poly (ether sulfone) porous hollow-fiber membrane formation. *Journal of Applied Polymer Science*, **2008**, 108(5), 3411-3418.
[3] Arahman, N., Maruyama, T., Sotani, T., Matsuyama, H. Effect of hypochlorite treatment on performance of hollow fiber membrane prepared from polyethersulfone/n-methyl-2-pyrrolidone/tetronic 1307 solution. *Journal of Applied Polymer Science*, **2008**, 110(2), 687-694.
[4] Takagi, R., Mulyati, S., Arahman, N., Ohmukai, Y., Maruyama, T., Matsuyama, H. Time dependence of transport number ratio during electrodialysis process. *Desalination and Water Treatment*, **2011**, 34(1-3), 25-31.
[5] Arahman, N., Maimun, T., Bilad, M. Fabrication of polyethersulfone membranes using nanocarbon as additive. *GEOMATE Journal*, **2018**, 15(50), 51-57.
[6] Muhammad, S., Yahya, E.B., Abdul Khalil, H., Marwan, M., Albadn, Y.M. Recent advances in carbon and activated carbon nanostructured aerogels prepared from agricultural wastes for wastewater treatment applications. *Agriculture*, **2023**, 13(1), 208.
[7] Muhammad, S., Abdul Khalil, H., Abd Hamid, S., Albadn, Y.M., Suriani, A., Kamaruzzaman, S., Mohamed, A., Allaq, A.A., Yahya, E.B. Insights into agricultural-waste-based nano-activated carbon fabrication and modifications for wastewater treatment application. *Agriculture*, **2022**, 12(10), 1737.
[8] Macías-García, A., Carrasco-Amador, J., Encinas-Sánchez, V., Díaz-Díez, M., Torrejón-Martín, D. Preparation of activated carbon from kenaf by activation with h3po4. Kinetic study of the adsorption/electroadsorption using a system of supports designed in 3d, for environmental applications. *Journal of Environmental Chemical Engineering*, **2019**, 7(4), 103196.
[9] Azam, K., Shezad, N., Shafiq, I., Akhter, P., Akhtar, F., Jamil, F., Shafique, S., Park, Y.-K., Hussain, M. A review on activated carbon modifications for the treatment of wastewater containing anionic dyes. *Chemosphere*, **2022**, 306, 135566.
[10] Pet, I., Sanad, M.N., Farouz, M., ElFaham, M.M., El-Hussein, A., El-Sadek, M.A., Althobiti, R.A., Ioanid, A. Recent developments in the implementation of activated carbon as heavy metal removal management. *Water Conservation Science and Engineering*, **2024**, 9(2), 62.
[11] Togibasa, O., Dahlan, K., Ansanay, Y.O., Runggaweri, A.F., Merani, M. Surface modification of activated carbon from sago waste. *Journal of Metals, Materials and Minerals*, **2023**, 33(1), 95-100.
[12] Yousef, R., Qiblawey, H., El-Naas, M.H. Adsorption as a process for produced water treatment: A review. *Processes*, **2020**, 8(12), 1657.
[13] Zhao, C., Zhou, J., Yan, Y., Yang, L., Xing, G., Li, H., Wu, P., Wang, M., Zheng, H. Application of coagulation/flocculation in oily wastewater treatment: A review. *Science of the Total Environment*, **2021**, 765, 142795.
[14] Zaharia, C., Musteret, C.-P., Afrasinei, M.-A. The use of coagulation–flocculation for industrial colored wastewater treatment—(i) the application of hybrid materials. *Applied Sciences*, **2024**, 14(5), 2184.
[15] Tang, L., Zhang, S., Li, M., Zhang, X., Wu, Z., Ma, L. Numerical investigation on the dynamic flow pattern in a new wastewater treatment system. *Water*, **2021**, 13(8), 1101.
[16] Piaggio, A.L., Smith, G., de Kreuk, M.K., Lindeboom, R.E. Application of a simplified model for assessing particle removal in dissolved air flotation (daf) systems: Experimental verification at laboratory and full-scale level. *Separation and Purification Technology*, **2024**, 340, 126801.
[17] Santos, M.A., Capponi, F., Ataíde, C.H., Barrozo, M.A. Wastewater treatment using daf for process water reuse in apatite flotation. *Journal of Cleaner Production*, **2021**, 308, 127285.
[18] Khader, E.H., Muslim, S.A., Saady, N.M.C., Ali, N.S., Salih, I.K., Mohammed, T.J., Albayati, T.M., Zendehboudi, S. Recent advances in photocatalytic advanced oxidation processes for organic compound degradation: A review. *Desalination and Water Treatment*, **2024**, 318, 100384.
[19] Hübner, U., Spahr, S., Lutze, H., Wieland, A., Rüting, S., Gernjak, W., Wenk, J. Advanced oxidation processes for water and wastewater treatment–

guidance for systematic future research. *Heliyon*, **2024**, 10(9).
[20] Huang, J., Ran, X., Sun, L., Bi, H., Wu, X. Recent advances in membrane technologies applied in oil–water separation. *Discover Nano*, **2024**, 19(1), 66.
[21] Young, A.H., Hotz, N., Hawkins, B.T., Kabala, Z.J. Inducing deep sweeps and vortex ejections on patterned membrane surfaces to mitigate surface fouling. *Membranes*, **2024**, 14(1), 21.
[22] Mat Nawi, N.I., Bilad, M.R., Anath, G., Nordin, N.A.H., Kurnia, J.C., Wibisono, Y., Arahman, N. The water flux dynamic in a hybrid forward osmosis-membrane distillation for produced water treatment. *Membranes*, **2020**, 10(9), 225.
[23] Fathanah, U., Machdar, I., Riza, M., Arahman, N., Yusuf, M., Muchtar, S., Bilad, M.R., Md Nordin, N.A.H. Enhancement of antifouling of ultrafiltration polyethersulfone membrane with hybrid mg (oh) 2/chitosan by polymer blending. *Journal of Membrane Science and Research*, **2020**, 6(4), 375-382.
[24] Ambarita, A.C., Arahman, N., Mulyati, S. A synergistic approach to improving antifouling and antibacterial properties of ag/dbr/pes membrane. *South African Journal of Chemical Engineering*, **2024**, 48, 30-39.
[25] Seah, M.Q., Chua, S.F., Ang, W.L., Lau, W.J., Mansourizadeh, A., Thamaraiselvan, C. Advancements in polymeric membranes for challenging water filtration environments: A comprehensive review. *Journal of Environmental Chemical Engineering*, **2024**, 12(3), 112628.
[26] Fahrina, A., Arahman, N., Aprilia, S., Bilad, M.R., Silmina, S., Sari, W.P., Sari, I.M., Gunawan, P., Pasaoglu, M.E., Vatanpour, V. Functionalization of peg-agnps hybrid material to alleviate biofouling tendency of polyethersulfone membrane. *Polymers*, **2022**, 14(9), 1908.
[27] Barambu, N.U., Bilad, M.R., Bustam, M.A., Kurnia, K.A., Othman, M.H.D., Nordin, N.A.H.M. Development of membrane material for oily wastewater treatment: A review. *Ain Shams Engineering Journal*, **2021**, 12(2), 1361-1374.
[28] Politano, A., Al-Juboori, R.A., Alnajdi, S., Alsaati, A., Athanassiou, A., Bar-Sadan, M., Beni, A.N., Campi, D., Cupolillo, A., D'Olimpio, G. 2024 roadmap on membrane desalination technology at the water-energy nexus. *Journal of Physics: Energy*, **2024**, 6(2), 021502.
[29] Mulyati, S., Muchtar, S., Arahman, N., Meirisa, F., Syamsuddin, Y., Zuhra, Z., Rosnelly, C.M., Shamsuddin, N., Mat Nawi, N.I., Wirzal, M.D.H. One-pot polymerization of dopamine as an additive to enhance permeability and antifouling properties of polyethersulfone membrane. *Polymers*, **2020**, 12(8), 1807.
[30] Barambu, N.U., Bilad, M.R., Wibisono, Y., Jaafar, J., Mahlia, T.M.I., Khan, A.L. Membrane surface patterning as a fouling mitigation strategy in liquid filtration: A review. *Polymers*, **2019**, 11(10), 1687.
[31] Barambu, N.U., Peter, D., Yusoff, M.H.M., Bilad, M.R., Shamsuddin, N., Marbelia, L., Nordin, N.A.H., Jaafar, J. Detergent and water recovery from laundry wastewater using tilted panel membrane filtration system. *Membranes*, **2020**, 10(10), 260.
[32] Luo, J., Hu, Y., Guo, X., Wang, A., Lin, C., Zhang, Y., Wang, H., Wang, Y., Tang, X. Effect of in situ aeration on ultrafiltration membrane fouling control in treating seasonal high-turbidity surface water. *Water*, **2024**, 16(15), 2195.
[33] Rowshan, R., Mousavi, S.M., Saljoughi, E., Karkhanechi, H. Mitigation of fouling using pvc 3d printed composite membrane with the wavy surface. *Journal of Environmental Chemical Engineering*, **2024**, 12(2), 112090.
[34] Boivin, S., Fujioka, T. Membrane fouling control and contaminant removal during direct nanofiltration of surface water. *Desalination*, **2024**, 581, 117607.
[35] Lin, W., Wang, Q., Liu, Z., Meng, X., Dai, P., Huang, X. Improved hydrodynamic properties and enhanced resistance to particle deposition and membrane fouling by millimeter-scale patterned membranes. *Journal of Membrane Science*, **2024**, 700, 122709.
[36] Young, A.H., Hotz, N., Hawkins, B.T., Kabala, Z.J. Inducing deep sweeps and vortex ejections on patterned membrane surfaces to mitigate surface fouling. *Membranes*, **2024**, 14(1), 21.
[37] Chauhan, D., Kumar Nagar, P., Pandey, K., Pandey, H. Fouling mitigation by surface-patterned polymeric membranes in water treatment: A review of recent advancements in fabrication techniques. *Macromolecular Symposia*, **2024**, 413(1), 2300053.
[38] Chauhan, D., Nagar, P.K., Pandey, K., Pandey, H. Simulations of novel mixed-patterned membrane surfaces: Enhanced hydrodynamics and concentration polarization to mitigate fouling in water treatment. *Journal of Water Process Engineering*, **2024**, 62, 105371.
[39] Daddi-Moussa-Ider, A., Tjhung, E., Richter, T., Menzel, A.M. Hydrodynamics of a disk in a thin film of weakly nematic fluid subject to linear friction. *Journal of Physics: Condensed Matter*, **2024**, 36(44), 445101.
[40] Ibrahim, Y., Hilal, N. A critical assessment of surface-patterned membranes and their role in advancing membrane technologies. *ACS ES&T Water*, **2023**, 3(12), 3807-3834.

[41] Chauhan, D., Nagar, P.K., Pandey, K., Pandey, H. Simulations of novel mixed-patterned membrane surfaces: Enhanced hydrodynamics and concentration polarization to mitigate fouling in water treatment. *Journal of Water Process Engineering*, **2024**, 62, 105371.
[42] Zare, S., Kargari, A. State-of-the-art surface patterned membranes fabrication and applications: A review of the current status and future directions. *Chemical Engineering Research and Design*, **2023**, 196, 495-525.
[43] Wang, C., Ma, Z., Qiu, Y., Wang, C., Ren, L.-F., Shen, J., Shao, J. Patterned dense janus membranes with simultaneously robust fouling, wetting and scaling resistance for membrane distillation. *Water Research*, **2023**, 242, 120308.
[44] Dattabanik, S., Banik, I., Sasmal, H., Rana, K., Das, S., Sarkar, D. Application of turbulence promoter in protein recovery from food wastewater by dynamic shear enhanced ultrafiltration. *Journal of Water Process Engineering*, **2022**, 48, 102877.
[45] Thomas, N., Kumar, M., Palmisano, G., Al-Rub, R.K.A., Alnuaimi, R.Y., Alhseinat, E., Rowshan, R., Arafat, H.A. Antiscaling 3d printed feed spacers via facile nanoparticle coating for membrane distillation. *Water Research*, **2021**, 189, 116649.
[46] Kucera, J. Reverse Osmosis: Design, Processes, and Applications for Engineers. Wiley-Scrivener; **2010**.
[47] Koo, J.W., Ho, J.S., Tan, Y.Z., Tan, W.S., An, J., Zhang, Y., Chua, C.K., Chong, T.H. Fouling mitigation in reverse osmosis processes with 3d printed sinusoidal spacers. *Water Research*, **2021**, 207, 117818.
[48] Lin, W., Zhang, Y., Li, D., Wang, X.-m., Huang, X. Roles and performance enhancement of feed spacer in spiral wound membrane modules for water treatment: A 20-year review on research evolvement. *Water Research*, **2021**, 198, 117146.
[49] Tsai, H.Y., Huang, A., Luo, Y.L., Hsu, T.Y., Chen, C.H., Hwang, K.J., Ho, C.D., Tung, K.L. 3d printing design of turbulence promoters in a cross-flow microfiltration system for fine particles removal. *Journal of Membrane Science*, **2019**, 573, 647-656.
[50] Bhattacharjee, C., Saxena, V., Dutta, S. Static turbulence promoters in cross-flow membrane filtration: A review. *Chemical Engineering Communications*, **2020**, 207(3), 413-433.
[51] Jiang, B., Hu, B., Yang, N., Zhang, L., Sun, Y., Xiao, X. Study of turbulence promoters in prolonging membrane life. *Membranes*, **2021**, 11(4), 268.
[52] Wang, S., Wang, Z., Xia, J., Wang, X. Polyethylene-supported nanofiltration membrane with in situ formed surface patterns of millimeter size in resisting fouling. *Journal of Membrane Science*, **2021**, 620, 118830.
[53] Abdel-Aty, A.A., Ahmed, R.M., ElSherbiny, I.M., Panglisch, S., Ulbricht, M., Khalil, A.S. Superior separation of industrial oil-in-water emulsions utilizing surface patterned isotropic pes membranes. *Separation and Purification Technology*, **2023**, 311, 123286.
[54] Park, J.E., Jung, S.Y., Kang, T.G. Enhanced reverse osmosis filtration via chaotic advection induced by patterned membranes: A numerical study. *Desalination*, **2023**, 565, 116879.
[55] Wang, Q., Lin, W., Chou, S., Dai, P., Huang, X. Patterned membranes for improving hydrodynamic properties and mitigating membrane fouling in water treatment: A review. *Water Research*, **2023**, 236, 119943.
[56] Chevarin, C., Wang, X., Bouyer, D., Tarabara, V., Chartier, T., Ayral, A. Cfd-guided patterning of tubular ceramic membrane surface by stereolithography: Optimizing morphology at the mesoscale for improved hydrodynamic control of membrane fouling. *Journal of Membrane Science*, **2023**, 672, 121435.
[57] Wang, Q., Lin, W., Chou, S., Dai, P., Huang, X. Patterned membranes for improving hydrodynamic properties and mitigating membrane fouling in water treatment: A review. *Water Research*, **2023**, 236, 119943.
[58] Heinz, O., Aghajani, M., Greenberg, A.R., Ding, Y. Surface-patterning of polymeric membranes: Fabrication and performance. *Current Opinion in Chemical Engineering*, **2018**, 20, 1-12.
[59] Ilyas, A., Gebreyohannes, A.Y., Qian, J., Reynaerts, D., Kuhn, S., Vankelecom, I.F. Micro-patterned membranes prepared via modified phase inversion: Effect of modified interface on water fluxes and organic fouling. *Journal of Colloid and Interface Science*, **2021**, 585, 490-504.
[60] Armbruster, S., Stockmeier, F., Junker, M., Schiller-Becerra, M., Yüce, S., Wessling, M. Short and spaced twisted tapes to mitigate fouling in tubular membranes. *Journal of Membrane Science*, **2020**, 595, 117426.
[61] Al-Tayawi, A.N., Gulyás, N.S., Gergely, G., Fazekas, Á.F., Szegedi, B., Hodúr, C., Lennert, J.R., Kertész, S. Enhancing ultrafiltration performance for dairy wastewater treatment using a 3D printed turbulence promoter. *Environmental Science and Pollution Research*, **2023**, 30(50), 108907–108916.
[62] Toh, K.Y., Liang, Y.Y., Lau, W.J., Fimbres Weihs, G.A. A review of cfd modelling and performance metrics for osmotic membrane processes. *Membranes*, **2020**, 10(10), 285.

[63] Fimbres-Weihs, G., Wiley, D. Review of 3d CFD modeling of flow and mass transfer in narrow spacer-filled channels in membrane modules. *Chemical Engineering and Processing: Process Intensification*, **2010**, 49(7), 759-781.
[64] Lin, W., Zhang, Y., Li, D., Wang, X.-m., Huang, X. Roles and performance enhancement of feed spacer in spiral wound membrane modules for water treatment: A 20-year review on research evolvement. *Water Research*, **2021**, 198, 117146.
[65] Qian, X., Anvari, A., Hoek, E.M., McCutcheon, J.R. Advancements in conventional and 3d printed feed spacers in membrane modules. *Desalination*, **2023**, 556, 116518.
[66] Ibrahim, Y., Hilal, N. The potentials of 3d-printed feed spacers in reducing the environmental footprint of membrane separation processes. *Journal of Environmental Chemical Engineering*, **2023**, 11(1), 109249.
[67] Lin, W., Wang, Q., Liu, Z., Meng, X., Dai, P., Huang, X. Improved hydrodynamic properties and enhanced resistance to particle deposition and membrane fouling by millimeter-scale patterned membranes. *Journal of Membrane Science*, **2024**, 700, 122709.
[68] Foo, K., Liang, Y., Goh, P., Fletcher, D. Computational fluid dynamics simulations of membrane gas separation: Overview, challenges and future perspectives. *Chemical Engineering Research and Design*, **2023**, 191, 127-140.
[69] Chong, Y., Fletcher, D., Liang, Y. Cfd simulation of hydrodynamics and concentration polarization in osmotically assisted reverse osmosis membrane systems. *Journal of Water Process Engineering*, **2024**, 57, 104535.
[70] Liang, Y., Fletcher, D. Computational fluid dynamics simulation of forward osmosis (fo) membrane systems: Methodology, state of art, challenges and opportunities. *Desalination*, **2023**, 549, 116359.
[71] Oliveira Neto, G.L., Oliveira, N.G., Delgado, J.M., Nascimento, L.P., Magalhães, H.L., Oliveira, P.L.d., Gomez, R.S., Farias Neto, S.R., Lima, A.G. Hydrodynamic and performance evaluation of a porous ceramic membrane module used on the water–oil separation process: An investigation by cfd. *Membranes*, **2021**, 11(2), 121.
[72] Liang, Y., Toh, K., Weihs, G.F. 3d cfd study of the effect of multi-layer spacers on membrane performance under steady flow. *Journal of Membrane Science*, **2019**, 580, 256-267.
[73] Toh, K.Y., Liang, Y.Y., Lau, W.J., Fimbres Weihs, G.A. A review of cfd modelling and performance metrics for osmotic membrane processes. *Membranes*, **2020**, 10(10), 285.
[74] Rana, K., Sarkar, D. Hydrodynamic study of the single-stirred membrane filtration module: a CFD-based approach. *Turkish Journal of Computer and Mathematics Education (TURCOMAT)*, **2020**, 11(3), 1854–1860.
[75] Barambu, N.U., Bilad, M.R., Laziz, A.M., Nordin, N.A.H.M., Bustam, M.A., Shamsuddin, N., Khan, A.L. A wavy flow channel system for membrane fouling control in oil/water emulsion filtration. *Journal of Water Process Engineering*, **2021**, 44, 102340.
[76] Kwon, H.J. Use of COMSOL Simulation for Undergraduate Fluid Dynamics Course. *Proceedings of the 2012 ASEE Annual Conference & Exposition, San Antonio*, Texas, **2012**.
[77] Kaya, R., Deveci, G., Turken, T., Sengur, R., Guclu, S., Koseoglu-Imer, D.Y., Koyuncu, I. Analysis of wall shear stress on the outside-in type hollow fiber membrane modules by cfd simulation. *Desalination*, **2014**, 351, 109-119.
[78] Mazinani, S., Al-Shimmery, A., Chew, Y.J., Mattia, D. 3d printed fouling-resistant composite membranes. *ACS Applied Materials & Interfaces*, **2019**, 11(29), 26373-26383.
[79] Shang, W., Liu, W., Wang, W., Khanzada, N.K., Guo, J., Li, M., Li, X., Lao, J.-Y., Jeong, S.Y., Tso, C.Y. Facile synthesis of micro-eggette patterned nanofiltration membrane with enhanced anti-fouling and rejection performance. *Desalination*, **2023**, 555, 116524.
[80] Jung, S.Y., Won, Y.-J., Jang, J.H., Yoo, J.H., Ahn, K.H., Lee, C.-H. Particle deposition on the patterned membrane surface: Simulation and experiments. *Desalination*, **2015**, 370, 17-24.
[81] Lee, Y.K., Won, Y.-J., Yoo, J.H., Ahn, K.H., Lee, C.-H. Flow analysis and fouling on the patterned membrane surface. *Journal of Membrane Science*, **2013**, 427, 320-325.
[82] Shang, W., Yang, S., Liu, W., Wong, P.W., Wang, R., Li, X., Sheng, G., Lau, W., An, A.K., Sun, F. Understanding the influence of hydraulic conditions on colloidal fouling development by using the micro-patterned nanofiltration membrane: Experiments and numerical simulation. *Journal of Membrane Science*, **2022**, 654, 120559.
[83] Lyu, Z., Ng, T.C.A., Tran-Duc, T., Lim, G.J., Gu, Q., Zhang, L., Zhang, Z., Ding, J., Phan-Thien, N., Wang, J. 3d-printed surface-patterned ceramic membrane with enhanced performance in crossflow filtration. *Journal of Membrane Science*, **2020**, 606, 118138.
[84] Choi, W., Lee, C., Yoo, C.H., Shin, M.G., Lee, G.W., Kim, T.-S., Jung, H.W., Lee, J.S., Lee, J.-H. Structural tailoring of sharkskin-mimetic patterned reverse osmosis membranes for optimizing biofouling resistance. *Journal of Membrane Science*, **2020**, 595, 117602.

[85] Jang, J.H., Lee, J., Jung, S.Y., Choi, D.-C., Won, Y.J., Ahn, K.H., Park, P.K., Lee, C.H. Correlation between particle deposition and the size ratio of particles to patterns in nano-and micro-patterned membrane filtration systems. *Separation and Purification Technology*, **2015**, 156, 608-616.
[86] Lin, W., Wang, Q., Liu, Z., Meng, X., Dai, P., Huang, X. Improved hydrodynamic properties and enhanced resistance to particle deposition and membrane fouling by millimeter-scale patterned membranes. *Journal of Membrane Science*, **2024**, 700, 122709.
[87] Zhou, Z., Ling, B., Battiato, I., Husson, S.M., Ladner, D.A. Concentration polarization over reverse osmosis membranes with engineered surface features. *Journal of Membrane Science*, **2021**, 617, 118199.
[88] Liu, J., Liu, Z., Liu, F., Wei, W., Li, Z., Wang, X., Dong, C., Xu, X. The application of saw-tooth promoter for flat sheet membrane filtration. *Desalination*, **2015**, 359, 149-155.
[89] Barambu, N.U., Bilad, M.R., Shamsuddin, N., Samsuri, S., Nordin, N.A.H.M., Arahman, N. The combined effects of the membrane and flow channel development on the performance and energy footprint of oil/water emulsion filtration. *Membranes*, **2022**, 12(11), 1153.
[90] Barambu, N.U., Bilad, M.R., Huda, N., Nordin, N.A.H.M., Bustam, M.A., Doyan, A., Roslan, J. Effect of membrane materials and operational parameters on performance and energy consumption of oil/water emulsion filtration. *Membranes*, **2021**, 11(5), 370.
[91] Krstić, D.M., Höflinger, W., Koris, A.K., Vatai, G.N. Energy-saving potential of cross-flow ultrafiltration with inserted static mixer: Application to an oil-in-water emulsion. *Separation and Purification Technology*, **2007**, 57(1), 134-139.
[92] Li, L., Ding, L., Tu, Z., Wan, Y., Clausse, D., Lanoisellé, J.-L. Recovery of linseed oil dispersed within an oil-in-water emulsion using hydrophilic membrane by rotating disk filtration system. *Journal of Membrane Science*, **2009**, 342(1-2), 70-79.
[93] Mazinani, S., Al-Shimmery, A., Chew, Y.J., Mattia, D. 3d printed fouling-resistant composite membranes. *ACS Applied Materials & Interfaces*, **2019**, 11(29), 26373-26383.
[94] Ngene, I.S., Lammertink, R.G., Wessling, M., Van der Meer, W.G. Particle deposition and biofilm formation on microstructured membranes. *Journal of Membrane Science*, **2010**, 364(1-2), 43-51.
[95] Won, Y.-J., Jung, S.-Y., Jang, J.-H., Lee, J.-W., Chae, H.-R., Choi, D.-C., Ahn, K.H., Lee, C.-H., Park, P.-K. Correlation of membrane fouling with topography of patterned membranes for water treatment. *Journal of Membrane Science*, **2016**, 498, 14-19.
[96] Choi, D.-C., Jung, S.-Y., Won, Y.-J., Jang, J.H., Lee, J.-W., Chae, H.-R., Lim, J., Ahn, K.H., Lee, S., Kim, J.-H. Effect of pattern shape on the initial deposition of particles in the aqueous phase on patterned membranes during crossflow filtration. *Environmental Science & Technology Letters*, **2017**, 4(2), 66-70.
[97] Choi, W., Lee, C., Lee, D., Won, Y.J., Lee, G.W., Shin, M.G., Chun, B., Kim, T.-S., Park, H.-D., Jung, H.W. Sharkskin-mimetic desalination membranes with ultralow biofouling. *Journal of Materials Chemistry A*, **2018**, 6(45), 23034-23045.
[98] Lee, Y.K., Won, Y.-J., Yoo, J.H., Ahn, K.H., Lee, C.-H. Flow analysis and fouling on the patterned membrane surface. *Journal of Membrane Science*, **2013**, 427, 320-325.
[99] Harandi, H.B., Hu, J., Asadi, A., Sui, P.-C., Zhang, L., He, T. Experimental and theoretical analysis of scaling mitigation for corrugated pvdf membranes in direct contact membrane distillation. *Journal of Membrane Science*, **2023**, 686, 122001.
[100] Hu, J., Harandi, H.B., Chen, Y., Zhang, L., Yin, H., He, T. Anisotropic gypsum scaling of corrugated polyvinylidene fluoride hydrophobic membrane in direct contact membrane distillation. *Water Research*, **2023**, 244, 120513.
[101] Choi, J., Cho, M., Shin, J., Kwak, R., Kim, B. Electroconvective instability at the surface of one-dimensionally patterned ion exchange membranes. *Journal of Membrane Science*, **2024**, 691, 122256.
[102] Chang, M.-J., Zhu, W.-Y., Wang, H., Hui, Q., Chen, J.-L., Xie, H.-X., Liu, J. Patterned nanofibrous membrane via hot-pressing for enhanced solar thermal evaporation. *Materials Chemistry and Physics*, **2023**, 302, 127727.
[103] Hindson, W.A., James, S. Effects of surface modification on a proton exchange membrane for improvements in green hydrogen production. *International Journal of Hydrogen Energy*, **2024**, 49, 1040-1047.
[104] Hu, C., Lee, Y.J., Ma, Y., Zhang, X., Jung, S.W., Hwang, H., Cho, H.K., Kim, M.-G., Yoo, S.J., Zhang, Q. Advanced patterned membranes for efficient alkaline membrane electrolyzers. *ACS Energy Letters*, **2024**, 9(3), 1219-1227.